

## Strathprints Institutional Repository

Cheung, David and Schmid, Friederike (2004) *A density-functional theory study of the confined soft ellipsoid fluid*. *Journal of Chemical Physics*, 120 (19). ISSN 0021-9606

Strathprints is designed to allow users to access the research output of the University of Strathclyde. Copyright © and Moral Rights for the papers on this site are retained by the individual authors and/or other copyright owners. You may not engage in further distribution of the material for any profitmaking activities or any commercial gain. You may freely distribute both the url (<http://strathprints.strath.ac.uk/>) and the content of this paper for research or study, educational, or not-for-profit purposes without prior permission or charge.

Any correspondence concerning this service should be sent to Strathprints administrator: <mailto:strathprints@strath.ac.uk>

## A density-functional theory study of the confined soft ellipsoid fluid

David L. Cheung and Friederike Schmid

Citation: *J. Chem. Phys.* **120**, 9185 (2004); doi: 10.1063/1.1703522

View online: <http://dx.doi.org/10.1063/1.1703522>

View Table of Contents: <http://jcp.aip.org/resource/1/JCPSA6/v120/i19>

Published by the [American Institute of Physics](#).

---

### Additional information on *J. Chem. Phys.*

Journal Homepage: <http://jcp.aip.org/>

Journal Information: [http://jcp.aip.org/about/about\\_the\\_journal](http://jcp.aip.org/about/about_the_journal)

Top downloads: [http://jcp.aip.org/features/most\\_downloaded](http://jcp.aip.org/features/most_downloaded)

Information for Authors: <http://jcp.aip.org/authors>

## ADVERTISEMENT



**ALL THE PHYSICS  
OUTSIDE OF  
YOUR JOURNALS.**

www.physics-today.org  
**physics  
today**

# A density-functional theory study of the confined soft ellipsoid fluid

David L. Cheung and Friederike Schmid

*Theoretische Physik, Universität Bielefeld, D-33615 Bielefeld, Germany*

(Received 9 January 2004; accepted 19 February 2004)

A system of soft ellipsoid molecules confined between two planar walls is studied using classical density-functional theory. Both the isotropic and nematic phases are considered. The excess free energy is evaluated using two different *Ansätze* and the intermolecular interaction is incorporated using two different direct correlation functions (DCF's). The first is a numerical DCF obtained from simulations of bulk soft ellipsoid fluids and the second is taken from the Parsons–Lee theory. In both the isotropic and nematic phases the numerical DCF gives density and order parameter profiles in reasonable agreement with simulation. The Parsons–Lee DCF also gives reasonable agreement in the isotropic phase but poor agreement in the nematic phase. © 2004 American Institute of Physics. [DOI: 10.1063/1.1703522]

## I. INTRODUCTION

The behavior of fluids near surfaces and interfaces has attracted great interest in recent years. The presence of a surface breaks the translational symmetry of the fluid, leading to behavior radically different to that in the bulk. This is particularly true for liquid crystals.<sup>1</sup> Many applications for liquid crystalline materials rely on the ability to manipulate the preferred alignment through the action of an external field. This behavior is strongly influenced by coupling between the liquid crystal and bounding surfaces.

As may be expected from above, there have been many studies of liquid-crystal systems near surfaces. Experimental studies have been performed using methods such as scanning tunnelling microscopy,<sup>2</sup> atom force microscopy,<sup>3</sup> and NMR,<sup>4</sup> among others. There have also been simulation studies, using lattice models,<sup>5</sup> hard<sup>6,7</sup> or soft single site models,<sup>8</sup> and a few studies using atomistic models.<sup>9</sup> It has also been studied by the all commonly used theoretical methods in liquid-crystal science. Both elastic theory and Landau–de Gennes<sup>10</sup> theory have been applied to this. However, the former makes some assumptions (e.g., slow director variation) that are invalid near a solid substrate, while the latter introduces phenomenological parameters that are not easily related to microscopic properties. Last, there have been several studies using density-functional theory (DFT),<sup>6,7,11–13</sup> or integral equation methods.<sup>14,15</sup>

In this paper we study a liquid-crystal fluid near a solid substrate using DFT.<sup>16,17</sup> DFT in principle provides a route to the thermodynamic properties of a fluid from knowledge of its microscopic (molecular) properties. The intermolecular potential is incorporated through the excess free-energy functional. While the exact form of this is unknown a number of approximations to this are commonly used, such as Onsager theory<sup>18</sup> and Parsons–Lee theory.<sup>19–21</sup>

Previous DFT calculations for liquid-crystalline systems have been hindered as the exact direct correlation function (DCF) is unknown. Commonly, this is approximated by the Mayer  $f$  function,

$$f(\mathbf{r}_{12}, \mathbf{u}_1, \mathbf{u}_2) = \exp\{-\beta V(\mathbf{r}_{12}, \mathbf{u}_1, \mathbf{u}_2)\} - 1, \quad (1)$$

where  $V(\mathbf{r}_{12}, \mathbf{u}_1, \mathbf{u}_2)$  is the intermolecular potential and  $\beta = 1/k_B T$  is the inverse temperature.  $\mathbf{r}_{12}$  and  $\mathbf{u}_1$  are the intermolecular vector and the orientation vector of molecule 1, respectively. For a hard potential, for which DFT calculations have mostly been limited to, the integral of the Mayer function gives the excluded volume between two particles.

However, recently the DCF has been calculated for the soft ellipsoid model for a number of state points in both the nematic and isotropic phase.<sup>22–24</sup> It has been shown to reproduce the bulk properties of the nematic fluid such as the elastic constants.<sup>22</sup> Thus it is hoped that this may provide a good description of the structure of the inhomogeneous fluid.

In this paper we consider one of the simplest situations: a fluid of ellipsoidal molecules interacting with a structureless wall. Both isotropic and nematic phases are considered. The paper is arranged as follows: In the next two sections the theory (Sec. II) and computational method are outlined (Sec. III). The results are then given in Sec. IV and a short summary follows in Sec. V.

## II. THEORY

### A. Density-functional theory

For a system of uniaxial molecules the grand potential can be written as

$$\begin{aligned} \beta\Omega[\rho(\mathbf{r}, \mathbf{u})] &= \beta F_{\text{id}}[\rho(\mathbf{r}, \mathbf{u})] + \beta F_{\text{ex}}[\rho(\mathbf{r}, \mathbf{u})] \\ &+ \beta \int d\mathbf{r} d\mathbf{u} V_{\text{ext}}(\mathbf{r}, \mathbf{u}) \rho(\mathbf{r}, \mathbf{u}) \\ &- \beta \mu \int d\mathbf{r} d\mathbf{u} \rho(\mathbf{r}, \mathbf{u}), \end{aligned} \quad (2)$$

where  $\rho(\mathbf{r}, \mathbf{u})$  is the orientationally dependent single-particle density distribution,  $V_{\text{ext}}(\mathbf{r}, \mathbf{u})$  is the external potential, and  $\mu$  is the chemical potential.  $F_{\text{id}}[\rho(\mathbf{r}, \mathbf{u})]$  and  $F_{\text{ex}}[\rho(\mathbf{r}, \mathbf{u})]$  are the ideal and excess free energies, respectively. The ideal free energy is given by

$$\beta F_{\text{id}}[\rho(\mathbf{r}, \mathbf{u})] = \int d\mathbf{r} d\mathbf{u} \rho(\mathbf{r}, \mathbf{u}) [\ln[\lambda^3 \rho(\mathbf{r}, \mathbf{u})] - 1], \quad (3)$$

where  $\lambda$  is the thermal de Broglie wavelength. The excess free energy is in general unknown. Here we use two *Ansätze* for  $F_{\text{ex}}[\rho(\mathbf{r}, \mathbf{u})]$ . In the first  $F_{\text{ex}}[\rho(\mathbf{r}, \mathbf{u})]$  is in the spirit of Onsager theory,<sup>17,18</sup>

$$\beta F_{\text{ex}}[\rho(\mathbf{r}, \mathbf{u})] = -\frac{1}{2} \int d\mathbf{r}_1 d\mathbf{u}_1 d\mathbf{r}_2 d\mathbf{u}_2 c(\mathbf{r}_{12}, \mathbf{u}_1, \mathbf{u}_2) \times \rho(\mathbf{r}_1, \mathbf{u}_1) \rho(\mathbf{r}_2, \mathbf{u}_2), \quad (4)$$

where  $c(\mathbf{r}_{12}, \mathbf{u}_1, \mathbf{u}_2)$  is the direct correlation function.

In the second  $F_{\text{ex}}[\rho(\mathbf{r}, \mathbf{u})]$  is taken to be a density expansion around the homogenous fluid with density  $\rho_0(\mathbf{u})$  truncated at the second-order term,<sup>25</sup>

$$\begin{aligned} \beta F_{\text{ex}}[\rho(\mathbf{r}, \mathbf{u})] = & - \int d\mathbf{r}_1 d\mathbf{u}_1 c^{(1)}(\mathbf{u}_1) [\rho(\mathbf{r}_1, \mathbf{u}_1) - \rho_0(\mathbf{u})] \\ & - \frac{1}{2} \int d\mathbf{r}_1 d\mathbf{u}_1 d\mathbf{r}_2 d\mathbf{u}_2 c(\mathbf{r}_{12}, \mathbf{u}_1, \mathbf{u}_2) \\ & \times \{\rho(\mathbf{r}_1, \mathbf{u}_1) - \rho_0(\mathbf{u}_1)\} \\ & \times \{\rho(\mathbf{r}_2, \mathbf{u}_2) - \rho_0(\mathbf{u}_2)\}, \end{aligned} \quad (5)$$

where  $\rho_0(\mathbf{u})$  is the density for the bulk, homogenous fluid and  $c^{(1)}(\mathbf{u})$  is the first-order direct correlation function. This can be identified with the excess chemical potential ( $\beta\mu_{\text{ex}} = -c^{(1)}$ ).<sup>25</sup>

For fixed external and chemical potentials, the equilibrium single-particle density is that which minimizes the grand potential. This is a solution to the Euler–Lagrange equation,

$$\frac{\delta\Omega[\rho(\mathbf{r}, \mathbf{u})]}{\delta\rho(\mathbf{r}, \mathbf{u})} = 0, \quad (6)$$

$$\ln\{\lambda^3 \rho(\mathbf{r}, \mathbf{u})\} - \beta\mu(\mathbf{u}) + \beta V(\mathbf{r}, \mathbf{u}) + \frac{\delta\{\beta F_{\text{ex}}[\rho(\mathbf{r}, \mathbf{u})]\}}{\delta\rho(\mathbf{r}, \mathbf{u})} = 0. \quad (7)$$

The chemical potential is found from the Euler–Lagrange equation of the bulk, homogeneous fluid, i.e., substituting  $\rho(\mathbf{r}, \mathbf{u}) = \rho_0(\mathbf{u})$  into Eq. (7) for both *Ansätze* for the excess free energy.

The external potential is given by a repulsive Lennard–Jones potential,

$$V_{\text{ext}}(z) = \begin{cases} 4 \left[ \left( \frac{1}{z+0.5} \right)^{12} - \left( \frac{1}{z+0.5} \right)^6 \right] + 1, \\ \text{if } z < 2^{1/6} - 0.5, \\ 0, \text{ otherwise.} \end{cases} \quad (8)$$

This potential acts upon the molecular centres, thus giving rise to homeotropic (normal) alignment at the surface.

## B. Direct correlation function

The direct correlation function (DCF),  $c(\mathbf{r}_{ij}, \mathbf{u}_i, \mathbf{u}_j)$ , is the central quantity in many theories of liquids and liquid crystals. For liquid-crystalline systems the simplest approximation to the DCF is that of Onsager where the DCF is taken

to be the Mayer  $f$  function. This corresponds to truncating the virial expansion at the second term, and thus is valid only for low densities and large elongations.

In this paper, two different forms of the DCF are considered. The first is a numerical DCF calculated from simulations of soft ellipsoid molecules.<sup>22–24</sup> In principle this should be an exact representation of the interactions within the fluid.

The second form is taken from Parsons–Lee theory.<sup>19–21</sup> This corresponds to a resummed virial series truncated, as in Onsager theory, at the second-order term. Thus the Parsons–Lee DCF is the Mayer  $f$  function multiplied by a density-dependent prefactor,

$$c^{\text{PL}}(\mathbf{r}_{12}, \mathbf{u}_1, \mathbf{u}_2) = \frac{\eta(4-3\eta)}{(1-\eta)^2} f(\mathbf{r}_{12}, \mathbf{u}_1, \mathbf{u}_2), \quad (9)$$

where  $\eta = \rho v_{\text{mol}}$  is the packing fraction. To calculate the Mayer function the intermolecular potential is required. For the soft ellipsoids considered in this paper, the potential is given by

$$\begin{aligned} V(\mathbf{r}_{12}, \mathbf{u}_1, \mathbf{u}_2) = & 4 \left[ \left( \frac{\sigma_0}{r_{12} - \sigma(\hat{\mathbf{r}}_{12}, \mathbf{u}_1, \mathbf{u}_2) + \sigma_0} \right)^{12} \right. \\ & \left. - \left( \frac{\sigma_0}{r_{ij} - \sigma(\hat{\mathbf{r}}_{12}, \mathbf{u}_1, \mathbf{u}_2) + \sigma_0} \right)^6 \right], \end{aligned} \quad (10)$$

where

$$\begin{aligned} \sigma(\hat{\mathbf{r}}_{ij}, \mathbf{u}_i, \mathbf{u}_j) = & \sigma_0 \left[ 1 - \frac{\chi}{2} \left\{ \frac{(\hat{\mathbf{r}}_{ij} \cdot \mathbf{u}_i + \hat{\mathbf{r}}_{ij} \cdot \mathbf{u}_j)^2}{1 + \chi \mathbf{u}_i \cdot \mathbf{u}_j} \right. \right. \\ & \left. \left. + \frac{(\hat{\mathbf{r}}_{ij} \cdot \mathbf{u}_i - \hat{\mathbf{r}}_{ij} \cdot \mathbf{u}_j)^2}{1 - \chi \mathbf{u}_i \cdot \mathbf{u}_j} \right\} \right]^{-1/2}, \end{aligned} \quad (11)$$

and  $\chi = (\kappa^2 - 1)/(\kappa^2 + 1)$ , where  $\kappa$  is molecular length-to-breadth ratio, equal to 3 for the system considered here.

In both theories the DCF is taken to be that of the bulk, homogeneous fluid (i.e., the density in the prefactor in Eq. (9) is fixed to be the bulk density). Extension of Parsons–Lee theory to inhomogeneous densities (i.e., a prefactor that depends on the spatially varying density) is possible although nontrivial<sup>26–28</sup> and application of this is beyond the scope of this paper.

## III. METHOD

Following Allen,<sup>6,7,29</sup> angular-dependent functions are expanded in spherical harmonics. The single-particle density and its logarithm become

$$\rho(\mathbf{r}, \mathbf{u}) = \sum_{l,m} \rho_{lm}(\mathbf{r}) Y_{lm}^*(\mathbf{u}) \quad (12)$$

and

$$\ln\{\lambda^3 \rho(\mathbf{r}, \mathbf{u})\} = \sum_{l,m} \tilde{\rho}_{lm}(\mathbf{r}) Y_{lm}(\mathbf{u}). \quad (13)$$

The use of the complex conjugate in Eq. (12) ensures  $\rho(\mathbf{r}, \mathbf{u}) \ln\{\lambda^3 \rho(\mathbf{r}, \mathbf{u})\} = \sum_{l,m} \rho_{lm}(\mathbf{r}) \tilde{\rho}_{lm}(\mathbf{r})$ .

Similarly, the direct correlation function is expanded as

$$c(\mathbf{r}_{12}, \mathbf{u}_1, \mathbf{u}_2) = \sum_{l_1, l_2, l, m_1, m_2, m} c_{l_1 m_1 l_2 m_2 l m} (r_{12}) \times Y_{l_1 m_1}(\mathbf{u}_1) Y_{l_2 m_2}(\mathbf{u}_2) Y_{lm}(\hat{\mathbf{r}}_{12}). \quad (14)$$

In the above sums,  $0 \leq l \leq l_{\max}$  and  $-l \leq m \leq l$ . Symmetry dictates that  $m_1 + m_2 + m = 0$  and that  $l_1, l_2$ , and  $l$  are even.

$$\frac{\beta\Omega[\rho(z, \mathbf{u})]}{A} = \int_0^L dz \sum_{l,m} \rho_{lm}(z) \{ \tilde{\rho}_{lm}(z) - \sqrt{4\pi} \delta_{l0} \} + \sum_{l,m} \beta \int_0^L dz V_{lm}(z) \rho_{lm}(z) - \sqrt{4\pi} \beta \mu \int_0^L dz \rho_{lm}(z) - \sum_{l_1, l_2, m} \frac{1}{2} \int_0^L dz_1 \int_0^L dz_2 C_{l_1 l_2 m}(|z_1 - z_2|) \rho_{l_1 m}(z_1) \rho_{l_2 \bar{m}}(z_2). \quad (15)$$

The  $V_{lm}(z)$  are the components of the spherical harmonics expansion of the external potential [ $V(z, \mathbf{u}) = \sum_{l,m} V_{lm}(z) Y_{lm}(\mathbf{u})$ ]. For the potential given above, the only nonzero term is  $V_{00}(z) = \sqrt{4\pi} V_{\text{ext}}(z)$ .

$C_{l_1 l_2 m}(z)$  is the integral of the DCF over  $r$  and  $\phi$  for a fixed  $z$ , given by

$$C_{l_1 l_2 m}(z) = \sum_l \sqrt{(2l+1)\pi} \int_z^\infty dr r c_{l_1 m l_2 \bar{m} l 0}(r) P_l\left(\frac{z}{r}\right), \quad (16)$$

where  $P_l(x)$  is the  $l$ th Legendre polynomial.

Similarly the grand potential for the second Ansatz becomes

$$\frac{\beta\Omega[\rho(z, \mathbf{u})]}{A} = \int_0^L dz \sum_{l,m} \rho_{lm} \{ \tilde{\rho}_{lm}(z) - \sqrt{4\pi} \delta_{l0} \} + \sum_{l,m} \beta \int_0^L dz V_{lm}(z) \rho_{lm}(z) - \sum_{l,m} \beta \mu_{lm} \int_0^L dz \rho_{lm}(z) - \frac{1}{2} \sum_{l_1, l_2, m} \int_0^L dz_1 \int_{-\infty}^\infty dz_2 C_{l_1 l_2 m}(|z_1 - z_2|) \rho_{l_1 m}(z_1) [\rho_{l_2 \bar{m}}(z_2) - 2\rho_{lm}^0] - \frac{1}{2} \sum_{l_1, l_2, m} \int_0^L dz_1 \int_{-\infty}^\infty dz_2 C_{l_1 l_2 m} \rho_{l_1 m}^0 \rho_{l_2 \bar{m}}, \quad (17)$$

where  $\mu_{lm} = \tilde{f}_l \delta_{m0}$  and  $\tilde{f}_l$  are the spherical harmonics coefficients of the logarithm of the bulk orientational distribution function. Note that here  $\mu$  includes contributions from the linear term in the excess free energy Eq. (5) and thus depends on orientation.

The equilibrium particle densities are found by tabulating the grand potential on a regular grid and then numerically minimizing Eq. (15) or Eq. (17) with respect to the  $\tilde{\rho}_{lm}(z)$ . This numerical minimization is performed using the conjugate gradients method.<sup>30</sup> The calculations were taken to be converged when the fractional change in energy between iterations was less than 0.001 (i.e.,  $E_{\text{new}} - E_{\text{old}} < 0.001 E_{\text{new}}$ ). Spatial integrals were evaluated using the trapezium rule with a grid spacing of 0.04, while angular integrations were performed using Gauss–Legendre quadrature with 800–6400 points.

Once the equilibrium orientationally dependent density  $\rho(z, \mathbf{u})$  is known, the bulk density can be calculated by integration over the angular variables, i.e.,

$$\rho_0(z) = \int d\mathbf{u} \rho(z, \mathbf{u}) = \sqrt{4\pi} \rho_{00}(z). \quad (18)$$

Similarly the second rank order parameter profile  $p_2(z)$  can be calculated from<sup>13</sup>

$$p_2(z) = \frac{\int d\mathbf{u} \rho(z, \mathbf{u}) P_2(\mathbf{u})}{\int d\mathbf{u} \rho(z, \mathbf{u})}, \quad (19)$$

$$p_2(z) = \frac{1}{\sqrt{5}} \frac{\rho_{20}(z)}{\rho_{00}(z)}.$$

## IV. RESULTS

### A. Density and order parameter profiles

#### 1. Isotropic phase

First we present results for calculations performed in the isotropic phase, with  $\rho^* = 0.24$  and  $T^* = 0.5$ . Shown in Fig. 1 are the density and order-parameter profiles obtained from

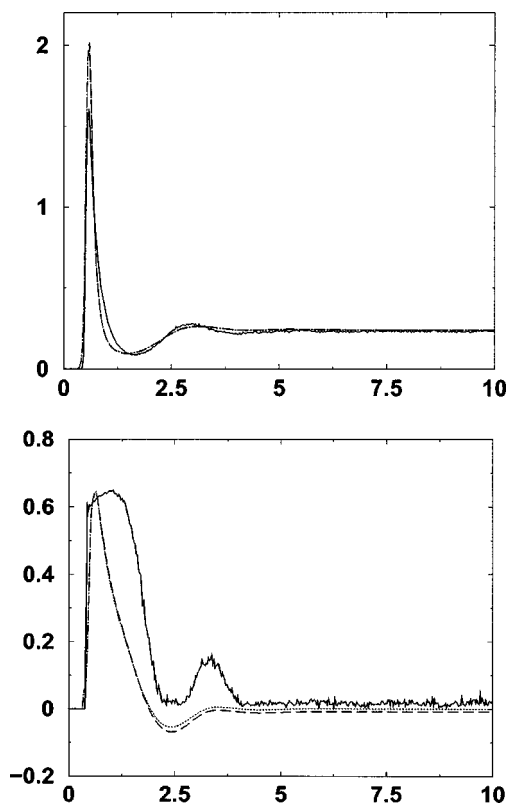


FIG. 1. (a) Density profiles for isotropic fluid with  $\rho^*=0.24$  and  $T^*=0.5$ . The solid line is the simulation data, the dashed line shows the data obtained from DFT calculations using Eq. (4) and the numerical DCF, and the dotted line shows the data obtained from DFT calculations using Eq. (5) and the numerical DCF. (b) Order-parameter profiles for isotropic fluid with  $\rho^*=0.24$  and  $T^*=0.5$ . Same symbols as in (a).

DFT calculations. Shown for comparison are profiles found from molecular-dynamics simulations of a confined system of soft ellipsoids.

As can be seen from Fig. 1(a) the density profiles found from DFT calculations using Eqs. (4) and (5) are virtually indistinguishable. The DFT profiles share the same gross features as those obtained from simulation. There is a strong maximum at about  $z=0.68$ , followed by a minimum at about  $z=1.44$ . There is also a weak maximum at about  $z=3.4$  in the DFT profiles and  $z=3$  in the simulation data. Both the DFT and simulation profiles rapidly tend towards the bulk density.

The most obvious difference between the DFT and simulation results is the height of the first peak. In the profile obtained from the DFT calculations the height of the first peak is about 2.02, while in the simulation data it is approximately 1.61.

Shown in Fig. 1(b) are the order-parameter profiles obtained from DFT calculations and simulation. As can be seen the agreement between the two profiles here is not as good as for the density. Both the DFT and simulation data have peaks at about  $z=0.64$ . This peak arises due to the effect of the surface on the ordering of the molecules. The heights of these peaks are both about  $p_2=0.64$ . This initial peak is then followed by a decrease in the order parameter.

In the DFT calculations the order parameter then becomes negative with a minimum at about  $z=2.4$ . The profile

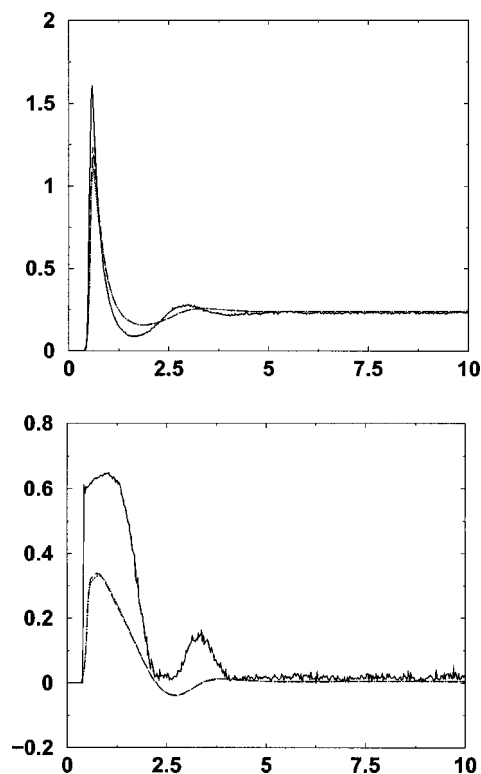


FIG. 2. (a) Density profiles for isotropic fluid with  $\rho^*=0.24$  and  $T^*=0.5$ . The solid line is the simulation data, the dashed line is data obtained from DFT calculations using Eq. (4) and the Parsons–Lee DCF, and the dotted line shows the density profile obtained from DFT calculations using Eq. (5) and the Parsons–Lee DCF. (b) Order-parameter profiles for isotropic fluid with  $\rho^*=0.24$  and  $T^*=0.5$ . Same symbols as in (a).

found from simulation has a minimum at about the same distance, although in this case the order parameter remains positive. Another maximum is present at about  $z=3.3$  in the simulation data. This is also present in the profiles obtained from DFT calculations, although of much smaller magnitude. Both profiles then rapidly decay to a constant value close to 0 indicating isotropic ordering in the bulk of the cell.

Shown in Fig. 2 are the density and order-parameter profiles obtained from DFT calculations using the Parsons–Lee DCF. As for those obtained using the numerical DCF, the density profiles [Fig. 2(a)] using Eqs. (4) and (5) are essentially identical and in good agreement with the profile obtained from simulation. Again a major discrepancy between the DFT and simulation profiles is the height of the first peak. In this case, however, the peak height is underestimated by the DFT calculations, 1.23 compared to 1.61 for the simulation profile.

The order-parameter profiles are shown in Fig. 2. As can be seen, the first peak in the order-parameter profiles obtained from DFT calculations is much smaller than in the simulation profile and those found from DFT calculations using the numerical DCF. For molecules with length-to-width ratio of 3, Parsons–Lee theory predicts an isotropic–nematic transition at about  $\rho=0.32$ ,<sup>21</sup> whereas for simulation the transition is at  $\rho=0.284$ . Thus for Parsons–Lee theory it is further from the nematic phase, and hence at lower order, than in simulation.

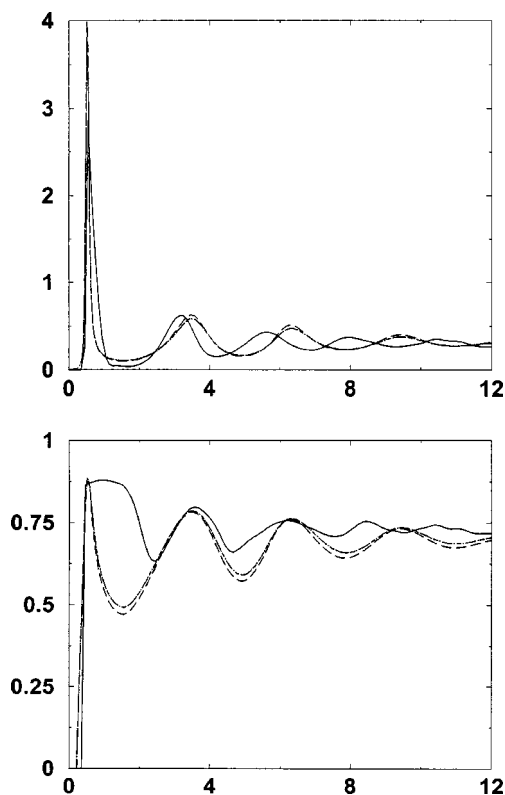


FIG. 3. (a) Density profiles for nematic fluid with  $\rho^*=0.30$  and  $T^*=0.5$ . The solid line is the simulation data, the dashed line is the data obtained from DFT calculations using Eq. (4) and numerical DCF, and the dotted line shows the data obtained from DFT calculations obtained from DFT calculations using Eq. (5) and the numerical DCF. (b) Order-parameter profiles for nematic fluid with  $\rho^*=0.30$  and  $T^*=0.5$ . Same symbols as in (a).

## 2. Nematic phase

Shown in Fig. 3 are the density and order-parameter profiles for the nematic phase ( $\rho^*=0.30$  and  $T^*=0.5$ ) calculated using DFT calculations and Monte Carlo simulation. In the simulations, the cell size was adjusted so that the average density in the cell bulk was 0.30 to aid comparison between simulation and theory. As can be seen the profiles obtained from DFT calculations using Eqs. (4) and (5) are in better agreement with each other than with the simulation profiles.

The density profiles are shown Fig. 3(a). As in the isotropic case, there is an initial peak in the density profile at about  $z=0.6$ . There are then further peaks. In the DFT profiles these subsequent peaks are at  $z=3.5$ ,  $z=6.3$ , and  $z=9.4$ . In the simulation profile, these are at  $z=3.2$ ,  $z=5.6$ , and  $z=7.9$ . A similar difference has been seen in comparison between DFT calculations and simulations for simple fluids.<sup>31,32</sup> This was explained due to the imposition of homogeneity in the transverse ( $x$  and  $y$ ) directions in the theoretical calculations.<sup>31</sup>

Aside from the positions of these secondary peaks, the other noticeable difference between the DFT and simulation profiles are in the heights of these peaks. As in the isotropic case the height of the initial peak is overestimated compared to simulation. The initial peak in the DFT calculations has a height of 3.9, while in the simulation profile its height is 2.9. In contrast to the isotropic phase, the secondary peaks in the DFT profile are more noticeable than those in the simulation

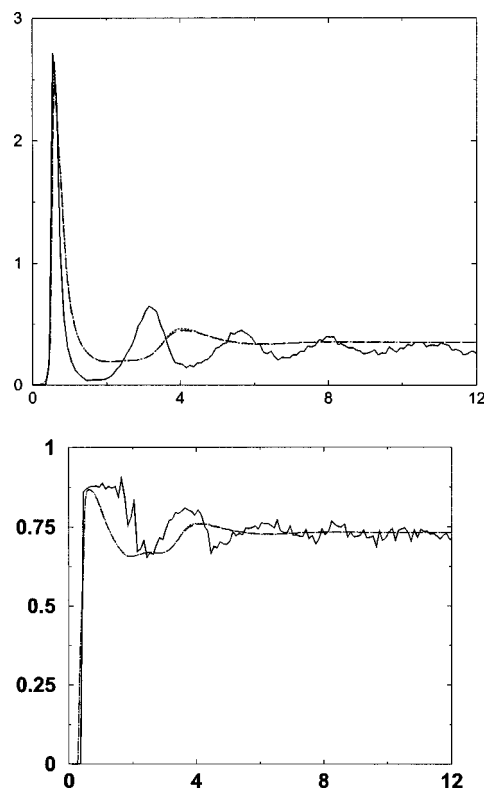


FIG. 4. (a) Density profiles for nematic fluid. The solid line is the simulation data ( $\rho^*=0.30$  and  $T^*=0.5$ ), the dashed line is data obtained from DFT calculations using Eq. (4) and Parsons-Lee DCF ( $\rho^*=0.35$  and  $T^*=0.5$ ), and the dotted line shows the data obtained from DFT calculations using Eq. (5) and Parsons-Lee DCF ( $\rho^*=0.35$  and  $T^*=0.5$ ). (b) Order-parameter profiles for nematic fluid. Same symbols as in (a).

profile. These secondary peaks are also stronger in the DFT profile calculated using Eq. (4) than those in the profile calculated using Eq. (5). These peaks indicate surface induced layering.<sup>1</sup> This has been observed in by x-ray reflectivity measurements, both at the nematic–solid interface as studied here and at the free nematic interface.

The second rank order parameter profiles are shown in Fig. 3(b). Again these show a strong initial peak at approximately  $z=0.6$ . This is then followed by a series of peaks before decaying to a bulk value as for the density profiles. These peaks are at approximately the same positions as the peaks in the density profiles. As for the density profile the secondary peaks are stronger than those in the simulation profile. In the center of the cell the DFT order parameters reach constant values. For Eq. (4) the order parameter in the center of the cell is 0.65, whereas for Eq. (5)  $p_2(z)=0.69$ . These values are close to the bulk of 0.69. The order parameter in the center of the cell from simulation is 0.74, higher than the bulk value.

One major difference between the DFT and simulation profiles is the decay of the initial peak. In the DFT profile there is a rapid decay from the first peak that is not seen in the simulation profile. This can also be seen, albeit not as dramatically, in the order-parameter profiles for the isotropic fluid (Figs. 1 and 2).

Shown in Fig. 4 are the density and order-parameter profiles calculated using the Parsons–Lee DCF and those from

simulation. For this model, Parsons–Lee theory predicts that a system with  $\rho^*=0.30$  is isotropic,<sup>21</sup> these calculations were performed with a higher bulk density ( $\rho^*=0.35$ ). While this difference makes detailed comparison impossible, it is small enough for qualitative comparison.

As can be seen, the density and order-parameter profiles calculated using Eqs. (4) and (5) are essentially identical and are similar to the profiles calculated in the isotropic phase using the Parsons–Lee DCF. This can be understood, as the Parsons–Lee DCF is proportional to the Mayer function at all densities, so aside from a constant the Parsons–Lee DCF is the same in both the isotropic and nematic phases. This leads to a lack of structure in the nematic density and order-parameter profiles compared to those from simulation and DCF calculations using the numerical DCF.

## B. Variable cell width

In this section, the effect of varying the width of the cell is examined. A fluid confined between two planar walls is often used in the evaluation of the depletion force between two colloidal particles.<sup>14</sup> Here the surface free energy  $\gamma$ , given by the excess (over bulk) grand potential per unit area,<sup>17</sup>

$$\beta\gamma = \frac{\beta\Omega[\rho(\mathbf{z}, \mathbf{u})] - \beta\Omega[\rho_0(\mathbf{u})]}{2A}, \quad (20)$$

is calculated for cell widths from 4 to  $40\sigma$ .

The surface free energy as a function of cell width is shown in Fig. 5. In all cases the it reaches a constant value for large cell widths (which is the surface tension). For large cell widths the walls become isolated from each other with a layer of bulk fluid intervening between the surface regions of fluid. At smaller cell widths there is no bulk fluid layer so the surface layers interact directly, leading to variation in the surface free energy with cell width. This behavior is generally oscillatory where the distance between peaks is of the order of the molecular length ( $2-3\sigma$ ).

Shown in Fig. 5(a) is the surface free energy as a function of cell width calculated using the numerical DCF. As can be seen the surface free for the nematic fluid is of larger magnitude than that of the isotropic fluid and shows much stronger variation with cell width. For the isotropic fluid it reaches a constant value for cell widths greater than about  $16\sigma$ . In contrast, in the nematic fluid it only approaches a constant value for cell widths greater than about  $25\sigma$ . This results from the larger range of the DCF in the nematic phase compared to in the isotropic phase.

Figure 5(b) shows the surface free energy as a function of cell width calculated using the Parsons–Lee DCF. As for the numerical DCF the surface free energy in the nematic phase is of greater magnitude and shows stronger variation with cell width than in the isotropic phase. In both the nematic and isotropic phases the it is constant for  $L$  greater than about  $18\sigma$ . This is in contrast to the behavior of the surface tension for the numerical DCF.

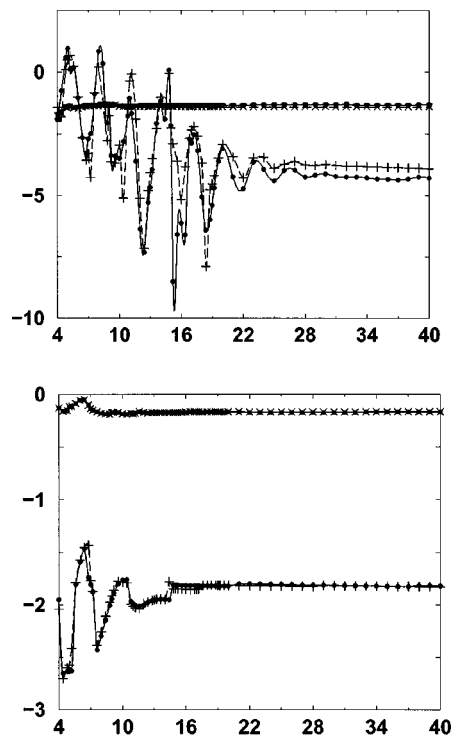


FIG. 5. (a) Variation of surface free energy with cell width calculated using the numerical DCF. The solid line with circles shows the energy of the isotropic fluid calculated using Eq. (4), the dashed line with circles shows the energy of the isotropic fluid calculated using Eq. (5), the solid line with squares shows the energy of the nematic fluid calculated using Eq. (4), and the dashed line with squares shows the energy of the nematic fluid calculated using Eq. (5). (b) Variation of the surface free energy with cell width calculated using the Parsons–Lee DCF. The solid line with circles shows the energy of the isotropic fluid calculated using Eq. (4), the dashed line with circles shows the energy of the isotropic fluid calculated using Eq. (5), the solid line with squares shows the energy of the nematic fluid calculated using Eq. (4), and the dashed line with squares shows the energy of the nematic fluid calculated using Eq. (5).

## V. SUMMARY

In this paper the structure of a fluid of soft ellipsoids near a soft wall is determined using density-functional theory calculations. The calculated density and order parameters have been compared to simulation results for the same system. Within the DFT calculations the excess free energy was obtained using both a numerical direct correlation function and a well-known approximation to the DCF. Two different *Ansätze* were used for the excess free energy, giving very similar results to each other.

There is qualitative agreement between the profiles found using the DFT method and those from simulation. The agreement is better in the isotropic phase, than for the nematic. In the isotropic case, the DFT calculations give profiles that appear to be less structured than those from simulation. This situation is reversed in the nematic phase.

For the isotropic phase, the Parsons–Lee DCF gave profiles similar to those from the numerical DCF. However, in the nematic phase the Parsons–Lee DCF gave profiles that were much less structured than those from the numerical DCF and simulation.

The variation in the surface free energy as a function of cell width has also been examined. For larger cell widths it is



a constant, whereas for small cell widths it reflects strong oscillatory interactions between the two surfaces.

In summary, the simple density functionals used in this paper, which are based on a second-order density expansion of the excess free energy, already give profiles which are in qualitative agreement with simulations. We still observe quantitative deviations, especially in the nematic phase. Therefore it will be interesting to compare these results with profiles obtained from more sophisticated density functionals, e.g., the Somoza–Tarazona functional<sup>26</sup> or the recently proposed modified Rosenfield functional.<sup>33</sup>

## ACKNOWLEDGMENTS

The authors wish to thank the German Science Foundation for funding. One of us (D.L.C.) is grateful to Enrique Velasco for helpful advice. The Monte Carlo program used was kindly provided by Mark Wilson.

<sup>1</sup>B. Jerome, Rep. Prog. Phys. **54**, 391 (1992).

<sup>2</sup>J. Frommer, Angew. Chem., Int. Ed. Engl. **31**, 1298 (1992).

<sup>3</sup>R. L. Williamson, M. Rivera, M. J. Miles, and K. D. Jandt, Proc. SPIE **2384**, 60 (1995).

<sup>4</sup>G. R. Luckhurst, P. J. Le Masurier, T. Miyamoto, K. Nakamura, T. H. Payne, A. Sugimara, and B. A. Timini, in *Proceedings of the 4th International Display Work-shop*, 1997.

<sup>5</sup>P. Pasini, C. Chiccoli, and C. Zannoni, in *Advances in the Computer Simulations of Liquid Crystals*, edited by P. Pasini and C. Zannoni (Kluwer, Dordrecht, 2000).

<sup>6</sup>M. P. Allen, Mol. Phys. **96**, 1391 (1999).

<sup>7</sup>D. Andrienko and M. P. Allen, Phys. Rev. E **65**, 021704 (2002).

<sup>8</sup>G. D. Wall and D. J. Cleaver, Phys. Rev. E **56**, 4306 (1997).

<sup>9</sup>D. J. Cleaver and D. J. Tildesley, Mol. Phys. **81**, 781 (1994).

<sup>10</sup>P. G. de Gennes and J. P. Prost, *Physics of Liquid Crystals*, 2nd edition, (Clarendon, Oxford, 1995).

<sup>11</sup>A. M. Somoza, L. Mederos, and D. E. Sullivan, Phys. Rev. E **52**, 5017 (1995).

<sup>12</sup>P. I. C. Teixeira, Phys. Rev. E **55**, 2876 (1997).

<sup>13</sup>A. Chrzanowska, P. I. C. Teixeira, H. Ehrentraut, and D. J. Cleaver, J. Phys.: Condens. Matter **13**, 4715 (2001).

<sup>14</sup>Y. Mao, M. E. Cates, and H. N. W. Lekkerkerker, J. Chem. Phys. **106**, 3721 (1997).

<sup>15</sup>Y. Mao, P. Bladon, H. N. W. Lekkerkerker, and M. E. Cates, Mol. Phys. **92**, 151 (1997).

<sup>16</sup>R. Evans, Adv. Phys. **28**, 143 (1979).

<sup>17</sup>J. P. Hansen and I. R. McDonald, *Theory of Simple Liquids*, 2nd edition (Academic, New York 1986).

<sup>18</sup>L. Onsager, Ann. N.Y. Acad. Sci. **51**, 627 (1949).

<sup>19</sup>J. D. Parsons, Phys. Rev. A **19**, 1225 (1979).

<sup>20</sup>S.-D. Lee, J. Chem. Phys. **87**, 4972 (1987).

<sup>21</sup>S.-D. Lee, J. Chem. Phys. **89**, 7036 (1988).

<sup>22</sup>N. H. Phuong, G. Germano, and F. Schmid, J. Chem. Phys. **115**, 7227 (2001).

<sup>23</sup>N. H. Phuong, G. Germano, and F. Schmid, Comput. Phys. Commun. **147**, 350 (2002).

<sup>24</sup>N. H. Phuong and F. Schmid, J. Chem. Phys. **119**, 1214 (2003).

<sup>25</sup>M. B. Sweatman, Mol. Phys. **98**, 573 (2000).

<sup>26</sup>A. Somoza and P. Tarazona, J. Chem. Phys. **91**, 517 (1989).

<sup>27</sup>H. Graf and H. Löwen, J. Phys.: Condens. Matter **11**, 1435 (1999).

<sup>28</sup>D. de las Heras, L. Mederos, and E. Velasco, Phys. Rev. E **68**, 031709 (2003).

<sup>29</sup>M. P. Allen, J. Chem. Phys. **112**, 5447 (2000).

<sup>30</sup>W. H. Press, B. P. Flannery, S. A. Teukolsky, and W. T. Vetterling, *Numerical Recipes* (Cambridge University Press, Cambridge, England, 1992).

<sup>31</sup>P. Tarazona, Phys. Rev. A **31**, 2672 (1985).

<sup>32</sup>T. K. Vanderlick, L. E. Scriven, and H. T. Davis, J. Chem. Phys. **90**, 2422 (1989).

<sup>33</sup>G. Cinacchi and F. Schmid, J. Phys.: Condens. Matter **14**, 12223 (2002).